

NATIONAL INSTITUTE FOR FUSION SCIENCE

Numerical Studies on Divertor Plasmas in Helical Systems

N. Ueda, K. Itoh and S.-I. Itoh

(Received — Aug. 30, 1989)

NIFS-2

Jan. 1990

RESEARCH REPORT NIFS Series

This report was prepared as a preprint of work performed as a collaboration research of the National Institute for Fusion Science (NIFS) of Japan. This document is intended for information only and for future publication in a journal after some rearrangements of its contents.

Inquiries about copyright and reproduction should be addressed to the Research Information Center, National Institute for Fusion Science, Nagoya 464-01, Japan.

NAGOYA, JAPAN

Numerical Studies on Divertor Plasmas in Helical Systems

Noriaki Ueda, Kimitaka Itoh⁺ and Sanae-I. Itoh⁺

Mitsubishi Atomic Power Industries, Inc.
4-1 Shibakouen 2-chome,
Minato-ku, Tokyo 105

⁺ National Institute for Fusion Science,
Chikusa-ku, Nagoya 464-01

Synopsis

Scrape-off layer and divertor plasmas in helical systems are studied by using the two-dimensional (2D) numerical simulation code. Unified Edge Divertor Analysis code (UEDA code) is applied to the straight helical model of torsatron/helical heliotron configurations. 2D profiles of plasma parameter, neutrals and impurities are obtained. Erosion rate and neutral back flow rate to the core plasma are also evaluated. Various shapes of the baffle plate are examined from the view point of the establishment of "dense-cold divertor plasma" by which we can avoid the damage of the target plate.

KEYWORDS: divertor, helical system, numerical simulation, dense-cold plasma, impurity.

§1. Introduction

Analysis on divertor and scrape-off layer (SOL) plasma has attracted attentions in recent researches on thermonuclear fusion.^{1, 2)} One motivation of the study on the divertor and SOL plasmas is to search for the proper method to control impurities and to realize the sufficient pumping of particles. The other motivation is the investigation on the improved confinement of the core plasma, which includes H-mode, improved Ohmic mode and so on.^{3, 4)} Experimental and theoretical studies have flourished, and detailed modellings have been developed. These modellings have been applied to a realistic geometry of tokamaks, and comparisons have been performed with considerable satisfaction.^{1, 2)} Several important key parameters, such as the connection length of the field line to the wall, have been identified.

The analysis on divertor and SOL plasmas has particular importance for toroidal helical systems such as stellarators.⁵⁾ For such configurations, the confining magnetic field is generated by the external winding current, not by the plasma current, so that the reality of stationary operation solely depends on the control of impurities and particles, not on the current sustainment. At the same time, fairly long confinement time for impurities has been reported for wide range of plasma parameters.⁶⁾ It is also noted that the connection length of the field line to the wall is much shorter than tokamaks with similar major radius,⁷⁾ so that the dense-and-cold divertor condition is hardly expected in helical systems. Considering the long impurity staying time

and short connection length of the field line to the wall, we note that it is inevitable to evaluate the efficiency of the divertor plasma from view point of reducing impurity sources for helical systems. It is also well known that the field line out of the plasma surface may be stochastic in these configurations.⁸⁾ It is necessary to explore the proper modelling of the plasma and magnetic field in SOL of the helical systems. The magnetic structure in the SOL and divertor plasma has recently been analyzed.^{7, 9)} The analysis clarify the effect of the short connection length (to the wall) on the boundary parameters.⁷⁾ The neutral particle behaviour is also solved by taking into account the plasma profile along the field line.¹⁰⁾

In studying the property of the SOL and divertor plasma, it is well known that the heat channel width is another key parameter.¹⁾ The knowledge on this width requires the 2D analysis. We, in this article, apply the Unifield Edge Divertor Analysis code^{11, 12)} (UEDA code) to the helical plasma. We employ the 2D model of torsatron/helical-heliotron configurations¹³⁾ with a realistic shape of baffle plate and rate of pumping. We obtain the 2D structures of the plasma, neutral particles and impurities in SOL and divertor regions. Erosion rate of the divertor plate is also calculated. Plasma size is close-to that of LHS. It is confirmed that the establishment of the dense-cold divertor plasma is generally difficult in this machine because of the short connection length of the field line to the wall. Emphasis is put on the study of the various shapes of the divertor chamber,

particularly the baffle plate. It is found that a careful choice of a complex configuration of the baffle plate can reduce the divertor temperature and increase the divertor density. Control of the pumping rate is found to be also effective to the behaviour of the edge/divertor plasma. Adequate considerations for the pumping rate would be required in the design of the divertor.

§2. Model

2.1 Model Geometry

We employ a simple model geometry of the $\ell=2$ torsatron/helical heliotron configurations (ℓ is the multipolarity of the field). A straight helical configuration is chosen and the separatrix magnetic surface is defined as the surface of the main plasma (see figure 1.). The up-down and right-left symmetries on the poloidal cross section is assumed. (The asymmetric structures of the plasma such as convective cell or MARFE¹⁴⁾ are out of the scope of this article.)

This model enables us the application of the 2D-time dependent numerical simulation code. The magnetic field structure of the SOL region has been studied.^{7, 9)} It was found that the connection length of the field line to the wall for the toroidal helical system is very close to the straight helical model in the case of torsatron/helical heliotron configurations, even though the stochastic region appears and separatrix magnetic surface disappears in the case of toroidal helical system.⁹⁾ We neglect the small magnetic islands in toroidal geometry. The plausibility of this assumption is discussed in §4.

The pitch of the field line, $B_{\text{poloidal}}/B_{\text{toroidal}}$ (B_p/B_t) is an important parameter of the analysis. In ref. [7], the average value B_p/B_t is discussed and is given as $c \cdot m / 2\pi l$, where m is the toroidal pitch number and c is a numerical coefficient of the order of unity. Averaged over the heat channel width, c is around 1/2 to 1. The connection length of the field line from the midplane to the wall has a dependence on the distance from the surface of the main plasma. This dependence is logarithmic, and the analytic calculation has shown that this dependence causes only small correction to the heat channel width and the plasma temperature.⁷⁾ We therefore neglect the logarithmic dependence and employ a simplified model of constant pitch parameter B_p/B_t .

2.2 Numerical Modelling

To simplify the problem, straight helical model (i.e., helical symmetry) is assumed and the quadrant model is employed as shown in Fig. 1. The orthogonal co-ordinates ψ and z , which correspond to the poloidal flux and the poloidal length of the magnetic field line of force are employed. In Fig. 1-(b), i and j denote the cell number in the z and ψ co-ordinates, respectively. The arc-length of the diverter, l , is measured along the plate on the poloidal cross section. In this figure, the solid line is the first wall (SUS) and the sheath plate is assumed to be made of graphite. The region between the first wall and the magnetic surface is assumed to be free from plasma particle, therefore only neutral transport

(by the Monte Carlo method) is solved. The section \overline{AB} is the inlet of the pumping duct. We regard the section as albedo surface (albedo value of 5%, i.e., 95% of impinging particles are reflected at the surface, is employed).

The reflection model at the material surface is the Eckstein/Verveek model for the graphite sheath plate and the Marlowe model for other structure.¹¹⁾ No wall pumping is assumed in the simulation, except the pumping at the section \overline{AB} as mentioned before.

The electron and ion energy inputs Q_e and Q_i from the core plasma to the SOL is set as $Q_e=Q_i=2.5$ MW and particle input Γ_p is assumed as $2 \times 10^{22} \text{ s}^{-1}$ in this quadrant model (This means that the total power out of the core plasma is 20 MW and particles of $8 \times 10^{22} \text{ s}^{-1}$).

2.3 Governing Fluid Equations

In the SOL and divertor regions, the two-fluid equations and the neutral gas transport are solved. A set of equations for the SOL and divertor plasma consists of the continuity equation for the density, the momentum conservation equation governing the parallel velocity $V_{||}$, the diffusion equation for the perpendicular velocity V_{ψ} with anomalous diffusion coefficient D_{ψ} (assumed as the Bohm diffusion) and the energy conservation equations for the electron and ion temperature T_e and T_i . We assumed the parallel conductivity is classical, and the model of $\chi_e=\chi_i=3 D_B$ is employed in the perpendicular one. The explicit forms of these equations are given in ref. [11] and are not repeated here.

3. Numerical Results

Numerical simulation is performed for given total plasma particle input $\Gamma_p = 8 \times 10^{22} \text{ s}^{-1}$ and heat input $Q_T (=Q_e + Q_i) = 20 \text{ MW}$. These values are chosen so that the particle confinement time $\tau_p = 10 \text{ msec}$ is satisfied for the averaged density $\bar{N}_e = 4 \times 10^{19} \text{ m}^{-3}$ ($\Gamma_p = \bar{N}_e V_p / \tau_p$) and the plasma volume, V_p , of 20 m^3 . The choice is consistent with experiments in present day helical devices.^{16, 17)} Throughout this paper, values are fixed in order to study the divertor performance for the given core plasma performance. The size of the plasma is as follows: major radius $R = 4 \text{ m}$ and $m = 10$ (i.e., helical pitch length is 2.51 m), $B_t = 4 \text{ T}$ at axis. The value of $\langle B_p / B_t \rangle$ is chosen as uniform value of 0.5 .⁷⁾ In this section, we first show the result for a standard divertor configuration which has a semi-closed divertor chamber bounded by the baffle plate. We examine the establishment of the dense and cold divertor plasma. The erosion rate of the divertor plate is calculated based on the physical sputtering process, and the influx of the carbon impurities is estimated. Based on the results of the standard case, we analyze two different divertor configurations in order to realize the better divertor performance. One is with the more closed divertor chamber (2nd model) and the other is with a fin structure (3rd model). Finally, the effect of the pumping rate on the divertor performance is also examined.

3.1 Standard Case

The spatial profiles of T_e and N_e , in the SOL and divertor region, are shown in Fig. 2-(a) and Fig. 2-(b). The

electron temperature T_e and density N_e are shown as a function of the poloidal length. The right hand edge corresponds to the divertor plate. The highest T_e and N_e are expected in the nearest flux tube ($j=5$) to the separatrix surface. The profile of the ion temperature T_i is similar to that of T_e . In this configuration, T_e at the mid-plane (T_e^b) is around 27 eV while at the divertor plate (T_e^d) is 12 eV. Because of the short connection length, the decrease of T_e at the divertor plate is expected to be small. N_e is about $3 \times 10^{19} \text{ m}^{-3}$ at the boundary and $9 \times 10^{19} \text{ m}^{-3}$ at the divertor plate. We do not observe the sufficient density buildup in front of the divertor plate. In fact, the multiplication factor of the particle flux at the divertor plate stays around 12, which shows that the particle recycling is insufficient in this divertor configuration. The results clearly show that the dense-and-cold divertor plasma is not established in this parameter range. Because of the high electron temperature at the divertor, the high erosion rate of the divertor plate is expected. In Fig. 3, we show the heat load and the erosion rate of the graphite plate. The electron heat flux, Q_e , the ion heat flux, Q_i , and the particle flux, Γ_d , are shown along the arc-length of the divertor plate. The peak values are observed in $j=5$ flux tube, each peak value is 272 W/cm^2 for Q_e , 270 W/cm^2 for Q_i and $1 \times 10^{24} \text{ s}^{-1}$ for integrated Γ_d . The graphite erosion rate associated with this load is calculated and is shown by the hatched region in Fig. 3. The high erosion rate is obtained and the highest rate of 120 cm/y is expected on $j=5$ flux tube. The erosion is due to the fuel ion

and the self-sputtering by carbon is negligibly small (about 2% of the total sputtering).

The sputtered carbon ions flow back to the main plasma through the SOL, if the shielding effect and the sputtering effect are insufficient. In Fig. 4, the contour plot of C^{4+} density is shown. Carbons are sputtered from the divertor plate, flow back to the SOL and would impinge into the core region. The dominant component of ionic carbons is C^{4+} , because of the temperature in the SOL. Its density reaches above $10^{18} m^{-3}$ near the midplane as is shown in Fig. 4. The total impinging flux of carbon ions to the main plasma is calculated to be $1.5 \times 10^{20} s^{-1}$, which may cause the radiation cooling near the edge as well as the dilution of fuel ions.

The particle pumping is found to be $4 \times 10^{22} s^{-1}$ in this case.

3.2 Study of Divertor Configurations

From the analysis in previous subsection, we see that the dense-and-cold divertor plasma is not established in a standard configuration. To search for the better configuration, we examine two different configuration of divertor chamber (2nd and 3rd models).

The 2nd configuration has the more closed divertor chamber and the 3rd one has the 'fin' structure in the chamber. The configurations are drawn in Fig. 5 together with the standard one.

For the same parameters as the standard case, we examine the divertor plasma performance. The results are listed on

Table 1. In table 1, the electron/ion temperatures at the midplane (T^b), those at the divertor plate (T^d), the density at the midplane (N^b) and the density at the divertor plate (N^d) as well as the multiplication factor of the particle flux at the divertor are compared. Also compared are the integrated neutral influx τ_{in}^0 to the main plasma and the peak values of erosion rate of the graphite plate.

From the view point of the establishment of dense-and-cold divertor plasma, the 2nd configuration (II) does not satisfy the condition. In spite of the tight baffle plate and the more closed divertor chamber, which is thought to be efficient for the density buildup, the expected density buildup is not observed. The pumping rate of neutral particles is enhanced as $6 \times 10^{22} s^{-1}$, and this leads to the reduction of the density in the SOL. As a result, the divertor temperature T_e^d becomes higher than that in case (I) (increase of the temperature at the midplane T_e^b is also observed in case (II)). The high erosion rate stays similar to case (I), since the increased sputtering yield ratio (because of the higher T_e^d) is compensated by the reduced incident particles. As a whole, we may say that the configuration (II) has little merit to the divertor performance in this parameter range.

The addition of a fin structure (III) is seen to have an effect on establishing the dense-and-cold divertor plasma. The density buildup near the divertor plate is seen as compared with cases (I) and (II). The flux multiplication factor is around 25 in this configuration, showing the sufficient recycling. The temperature at the divertor plate

is about 4 eV. Associated with this reduction, the erosion rate of the graphite decreases to only 0.1 m/y. We see sufficient divertor performance. In this case, the particle pumping is found to be $8 \times 10^{21} \text{ s}^{-1}$. Compared to the second case (II), the divertor density is 10 times larger but the particle pumping is small. This seems to be because of the screening of the recycling neutrals by the fin structure.

Another issue to be resolved in this configuration is the back flow rate of neutrals, τ_{in}^0 , to the main plasma. The ingress of neutrals to the main plasma will deteriorate the confinement properties. As is seen in Table 1, the back flow rate in case III, which is a most dense-cold plasma condition, shows the lesser value compared with the standard case (I). The back flow rate is the same level to the case II. This is because of the sufficient shielding of the neutral particles by the dense-cold plasma (small mean free path of neutrals) compared with the case I. It should also be noted the back flow rate is also affected by the pumping efficiency.

3.3 Effect of Pumping Efficiency

The pumping efficiency affects the divertor plasma performance. In case (I), we could not obtain the dense plasma near the divertor plate. This may be partly because of the high pumping rate. The pumping rate in the standard case is calculated to be $4 \times 10^{22} \text{ s}^{-1}$. To examine the effect of pumping efficiency, we reduce the pumping rate by a factor of 2 (by reducing the area of the pumping duct \overline{AB}), keeping the other parameters to be fixed in the standard configuration (I). The

results are summarized in the right hand column of Table 1. The reduction of the pumping rate causes the conspicuous increase of the divertor density, accordingly reduces the divertor temperature. Also, it is to be noted that the density in the SOL is higher than the standard case (I). The erosion rate of this case stays around 0.4 m/y, which seems to be a better one compared with the case (I) and case (II). The reduction of the pumping rate causes the back flow of neutrals to the SOL. Also, there is a possibility of increase of the influx of neutrals to the core plasma, Γ_{in}^0 . However, the numerical result does not show its increase in case (IV) compared with the case (I). This is because the density in the SOL as well as at the divertor region is higher in case (IV) than in case (I) as mentioned before and therefore, the mean free path of neutrals in case (IV) is shorter than in case (I). For this reason, Γ_{in}^0 in case (IV) stays $\sim 1 \times 10^{22} s^{-1}$ which is a similar value in case (I) though the pumped particles is a half of the case (I). In Fig. 6, comparison for the profiles of neutral density for cases (II), (III) and (IV) is shown. The neutral density in case (II) is low since a considerable amount of neutrals is pumped out. The retention of neutrals near the divertor plate is better in case (III) than in case (IV). But the neutral density in case (IV) is higher than in case (I) (see Fig. 2). From these results, we see that the pumping rate strongly affect the divertor performance.

§4. Summary and discussion

In this article we studied the SOL and divertor plasma in torsatron/helical heliotron configuration by using the Unified Edge Divertor Analysis code. The perpendicular and parallel transport coefficients are assumed to be Bohm like and classical, respectively.

For the LHS-grade plasma, we obtained the 2D profiles of the plasma, impurities and neutral particles for the given particle and heat fluxes from the core plasma. The erosion rate of the divertor plate was also calculated. Various shapes of the baffle plate were examined.

For the standard case of the simple baffle plate with $\Gamma_p = 8 \times 10^{22} \text{ s}^{-1}$ and $Q_T = 20 \text{ MW}$, the followings were found; the electron temperature at divertor plate T_e^d reaches 12 eV while that at the plasma boundary T_e^b remains 27 eV; the ratio N_e^d/N_e^b is about 3 and the flux enhancement factor Γ_d/Γ_p is 12, the erosion rate reaches about 1.2 m/y at the maximum. The motion of impurities was also solved and it was found that the carbon impurities flow to the main plasma. These features are not favourable from the view point of controlling the impurities and protection of the plate materials.

In order to resolve these difficulties, various shapes of complex baffle plate were examined. The second type of the baffle plate, i.e. the plate surrounds the SOL plasma near the throat, was found to enhance the pumping rate and to block the ionization in the throat region; the integrated particle flux to the divertor plate Γ_d , as a result, reduces to $3 \times 10^{23} \text{ s}^{-1}$ at

maximum. It was found that the divertor plasma density reduces and T_e^d increases to 33 eV. The reduction of Γ_d tends to reduce the erosion rate but the increase of the sputtering yield ratio compensates it. We found this type of the baffle plate is not the solution for the parameters studied here. The third type of the baffle plate is intended to increase the recycling near the divertor plate. This type was found to increase Γ_d ; T_d reaches $2 \times 10^{24} \text{ s}^{-1}$ at maximum and N^d/N^b becomes 10. By this improvement for Γ_d , the erosion rate was found to decrease to $\leq 0.1 \text{ m/y}$. It is noted that in this case the neutral back flow to the core plasma is $4 \times 10^{21} \text{ s}^{-1}$.

The effect of the pumping efficiency was also examined. The pumping efficiency was reduced to 1/2 for the case of the standard baffle plate. This can considerably improve the divertor condition (T_e^d decrease to 6 eV) reduced erosion rate ($\sim 0.4 \text{ m/y}$) without increase of the influx of neutrals to the core plasma compared with the standard case (I) at least for the assumed (Q_T, Γ_p).

The study on the case (IV) implies that the pumping speed is also effective on the establishment of the dense and cold divertor plasma. In this case, however, the electron density at plasma edge, N_b , reaches about $4.5 \times 10^{19} \text{ m}^{-3}$; this value can be comparable to the averaged plasma density of the core for this value of Γ_p , although the scaling law on the particle confinement time needs further refinement. This implies that the control of core density would be difficult in the case (IV). The compatibility with other requests for the core plasma should also be carefully studied.

From these studies, we summarize as follows;

- (1) very careful design is requested for the baffle plate in order to establish the dense-cold divertor plasma,
- (2) the baffle plate in the case (III) realizes the dense-cold plasma and reduces the erosion rate sufficiently (≤ 0.1 m/y),
- (3) the reduction of pumping efficiency in case (I) establish the dense-cold divertor plasma, though the influx of neutrals to the core plasma is higher than case (III)
- (4) screening of carbon impurity is not sufficient and therefore, carbon ions flow up to the core plasma.

It is noted that the calculation is performed for the fixed values of Γ_p and Q_T . As is well known, the reduction of Q_T and the increment of Γ_p can improve the divertor conditions. This means that the divertor condition imposes a constraint for the proper working region of the core-plasma. The search of this consistent working region for the core plasma is not in the scope of this article and is left for the future work.

We finally note that the simplified geometrical model is employed in this article. This is not a problem in dealing with the neutral particles because the mean free path in the plasma is much shorter than the toroidal curvature. One concern is the negligence of the fine structures, such as small magnetic islands, in the SOL region. We average out these three-dimensional structure and reduced the problem to the two-dimensional model. There is a possibility that this fine structure may cause a microscopic structure in the temperature profile: the most dangerous would be the narrow

peak of the heat flux to the divertor plate and very localized erosion on that plate. It is noted, however, there is a perpendicular diffusion across the magnetic surface, so that the sharpness of the heat channel is limited to a certain level; for the case of standard baffle plate, the heat width diffuses such that the half-width at half maximum across the field line reaches 4 mm. The structures finer than this length is averaged out by the diffusion. The diffusion coefficient is assumed to be Bohm-like. The absolute values obtained here depends on the diffusion model. The examination on the diffusion coefficient requires the comparison with experimental results in the present devices. It is also known that the drift heat flux, i.e., the $\vec{B} \times \nabla T$ term, affects the divertor functioning.^{2, 18)} Such an improvement of the model is also requested. These are left for the future research.

Acknowledgements

The authors acknowledge Drs. D.E. Post and A. Ehrhardt for their kind permission to use the DEGAS code. The computations have been made on CRAY-XMP.

The authors are very grateful to Drs. N. Ohyabu and T. Obiki for discussions on the LHS design parameters, to M. Tanaka (Century Research Centre Co.) for computer run, and M. Yamada, M. Nishikawa (Mitsubishi Atomic Power Ind. Inc.) for their support and to Dr. A. Iiyoshi for continuous encouragements. One of the authors (K.I.) acknowledges discussions with Drs. H. Zushi and T. Mizuuchi and Mr. K. Nagasaki.

This work has been partly supported by the Grant-in-Aid for Fusion Research and Grant-in-Aid for Scientific Research of the Japanese Ministry of Education.

References

- 1) See for instance, Physics of the Plasma Wall Interactions in Controlled Fusion (ed. D.E. Post and H. Behrisch, NATO ASI Series B131, Plenum Press, 1984) and papers quoted there in.
- 2) For recent progress, see for instance, Proceedings of the Eighth International Conference on Plasma-Surface Interactions in Controlled Fusion Devices (J. Nucl. Mater. 162-164 (1989)).
- 3) F. Wagner, et al., PRL 49 (1982) 1408.
- 4) F.X. Söldner, et al., Phys. Rev. Lett. 61 (1988) 1105.
- 5) L. Spitzer, Phys. Fluids 1 (1958) 253.
- 6) H. Kaneko and Heliotron E Group, Nucl. Fusion 27 (1987) 1075.
- 7) K. Itoh, et al., Nucl. Fusion 29 (1989) No.9 in press.
- 8) N. Filonenko, et al., Nucl. Fusion 7 (1967) 253.
- 9) K. Nagasaki, K. Itoh, to be published.
- 10) LHS group, "Next Large Helical Device (1988, March) Part III Section 2 (in Japanese).
- 11) N. Ueda, M. Kasai, M. Tanaka et al., Nucl. Fusion 28 (1988) 1183.
- 12) N. Ueda, K. Itoh, S.-I. Itoh, Nucl. Fusion 29 (1989) 173.
- 13) A.I. Morozov and L.S. Solov'ev, in Reviews of Plasma Physics (ed. M.A. Leontovich, Consultants Bureau, New York, 1966) vol. 2, p-1.
- 14) R. Lipschultz, B. LaBombard, E.S. Marmor, et al., Nucl. Fusion 24 (1988) 977.

- 15) D.B. Heifetz, J. Comput. Phys. 46 (1982) 309.
- 16) D. Okano, et al., J. Nucl. Materials, 145-147 (1987) 504.
- 17) K. Itoh et al., Report on the Grant-in-Aid for Fusion Research RF3(88)-1 "Problems in toroidal confinement" (in Japanese, 1988).
- 18) F.L. Hinton, Nucl. Fusion 25 (1985) 1457.
- 19) N. Ueda, K. Itoh, S.-I. Itoh et al., J. Nucl. Mater. 162-164 (1989) 607.

Figure Captions

Fig. 1 Poloidal Crosssection of the model geometry, (a)
Helical symmetry is assumed.

The surface of the main plasma is defined by the separatrix. The up-down and left-right symmetries are assumed. Analysis is done for the one quarter of the crosssection, (b).

The divertor plate (hatched) is assumed to be carbon and other solid surface is taken to be SUS. The thick line near the joint of the baffle plate indicate the location of the pumping duct, which is modeled by the albedo of 5%. Meshes and poloidal-radial indices are also shown.

Fig. 2 Profiles of the electron temperature and density in the SOL-divertor region, (a, b).

The index $j = 5$ indicate the magnetic surface touching the main plasma.

(c) illustrates the contour plot of the neutral particle distribution. In this case, the dense and cold divertor plasma is not established.

Fig. 3 Distributions on the divertor plate.

Abscissa is measured along the plate (see Fig. 1(b)).

Electron heat flux, ion heat flux and deuteron particle flux are shown. Erosion rate (averaged over small distance) is also shown by hatched histogram. The width (HWHM) of the heat channel is about 8 mm on the plate.

Fig. 4 Flow velocity of carbon impurities and the contour lines of the C^{4+} density. It is shown that the carbon impurities flow to the main plasma.

Fig. 5 Illustration of the baffle plates. One quarter of the poloidal crosssection is shown; Standard case (I), the closed divertor plate case (II) and the case with fin structure (III).

Fig. 6 Contour plot of neutral particle density for the cases of second (a) and third (b) types of baffle plates, respectively.

The case with reduced pumping is given in (c). The closed divertor plate enhances pumping and reduces the ionization in the SOL/divertor plasma. The fin structure (III) is effective in enhancing the recycling in divertor plasma.

Fig. 1

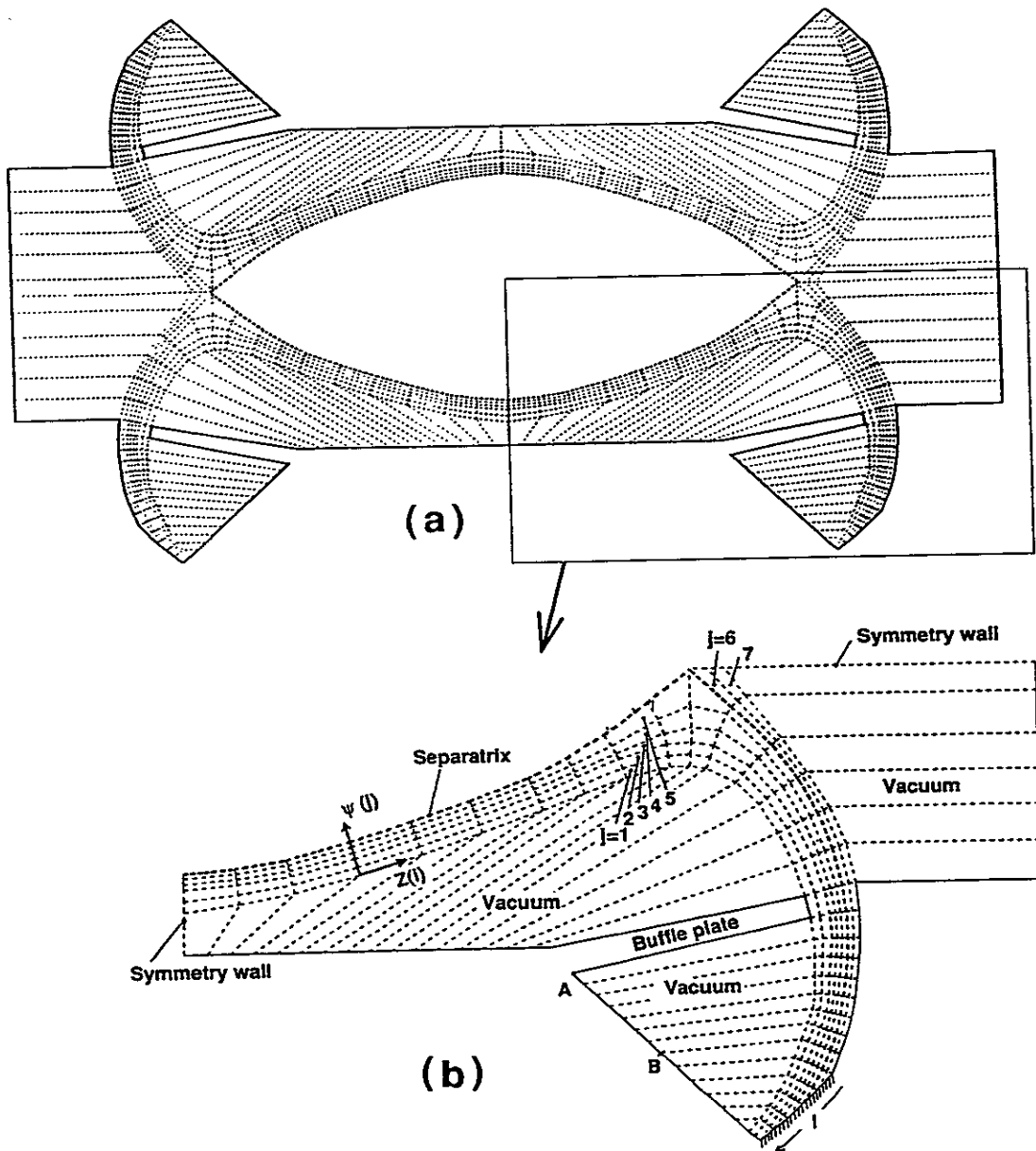


Fig. 2

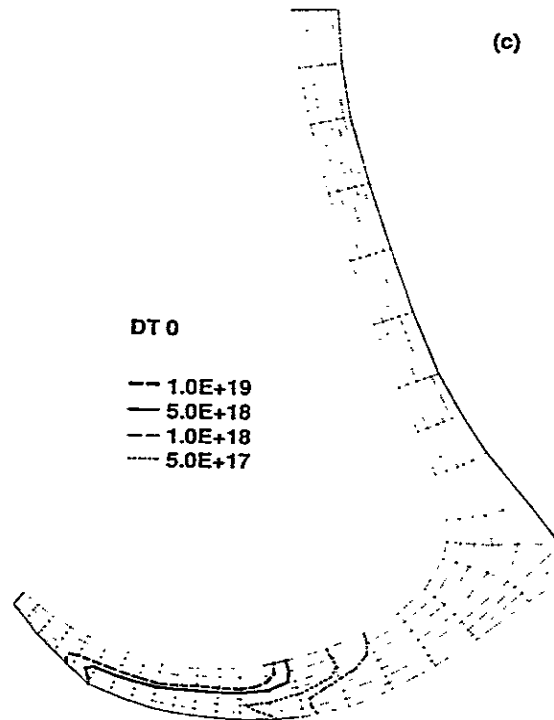
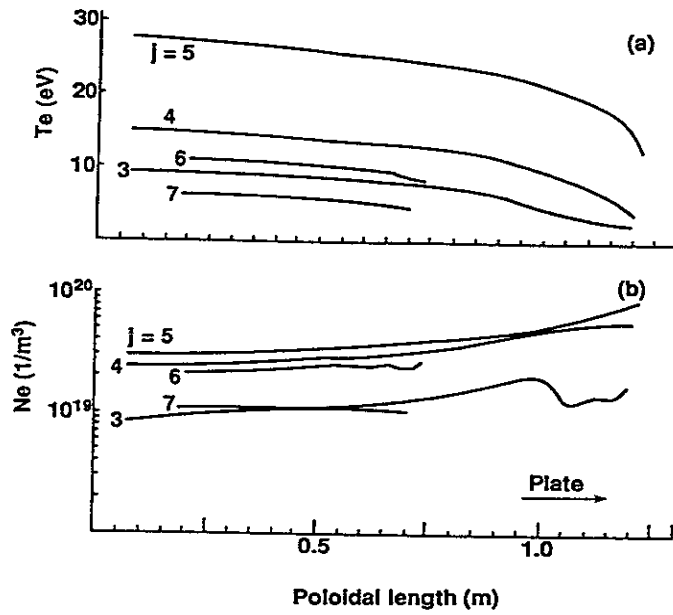


Fig. 3

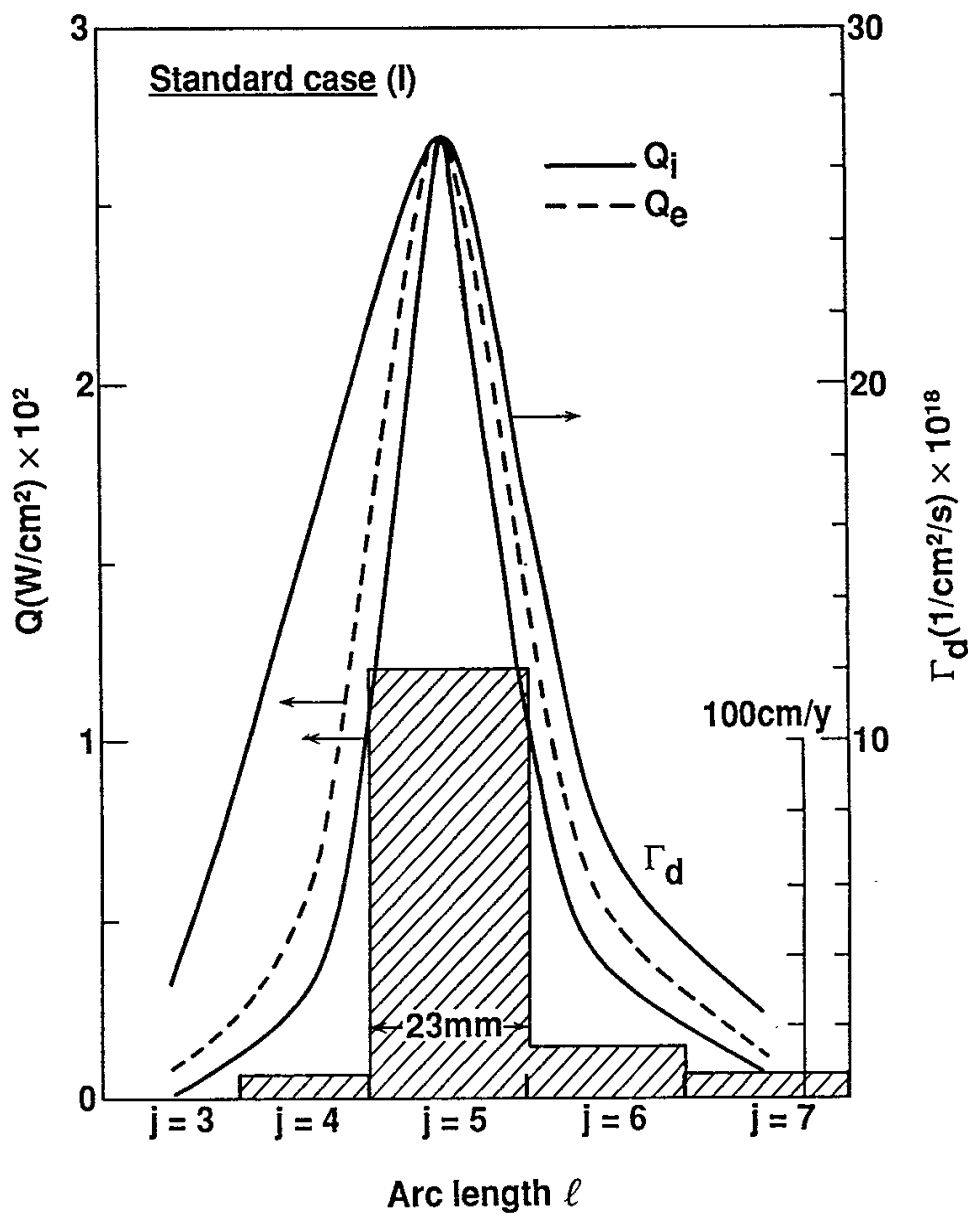


Fig. 4

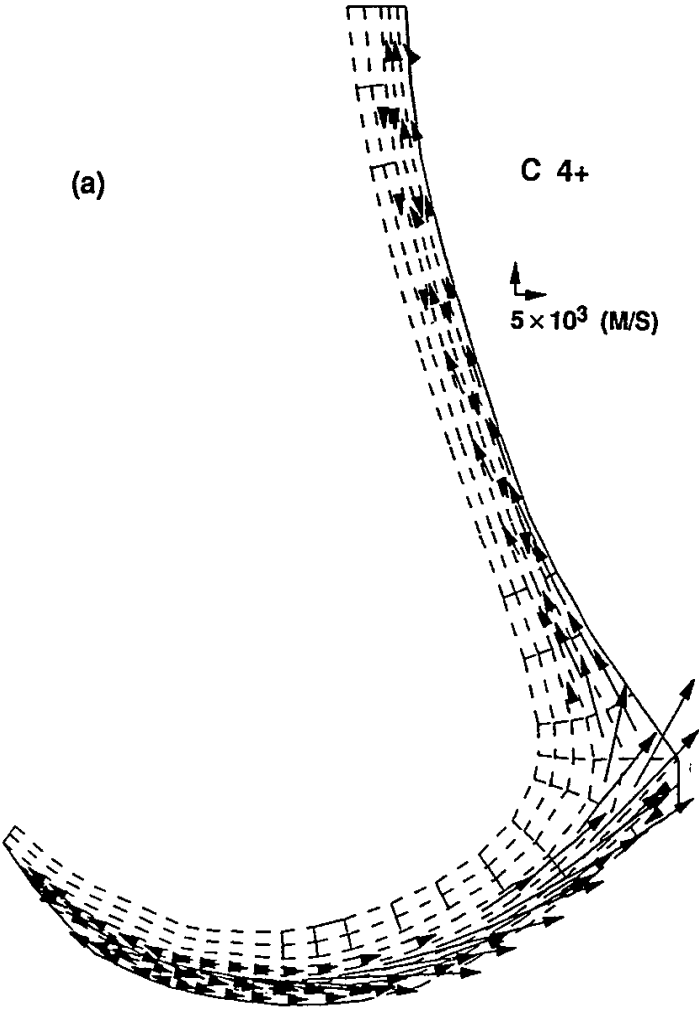


Fig. 4

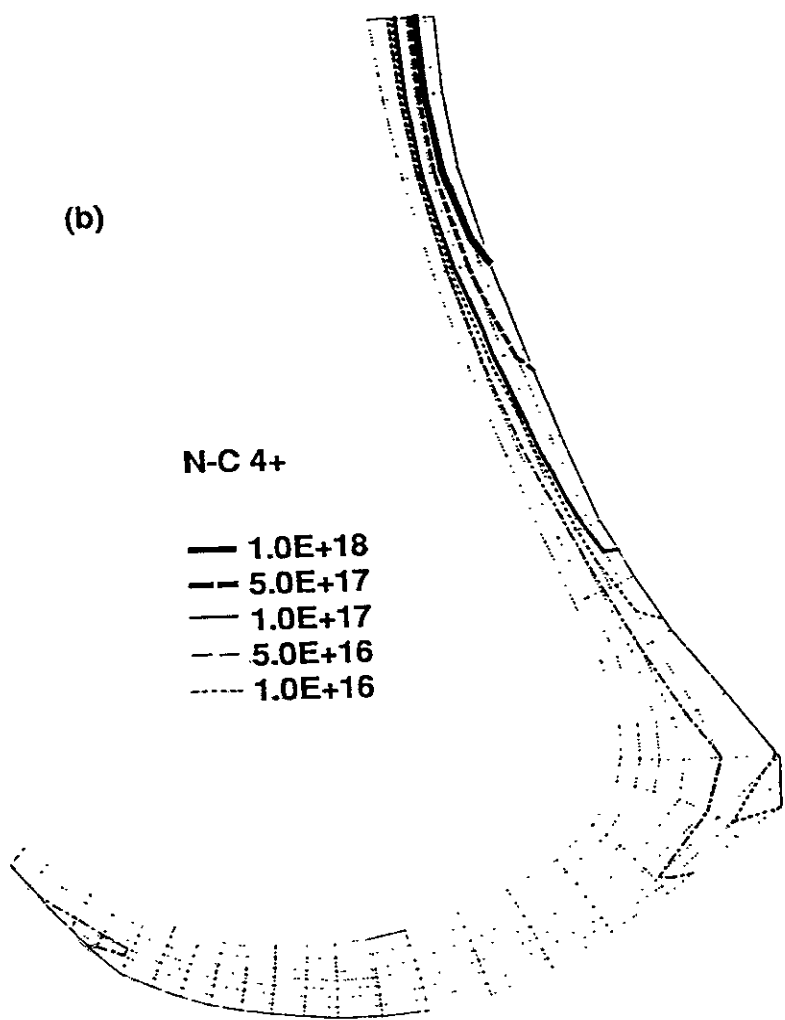


Fig. 5

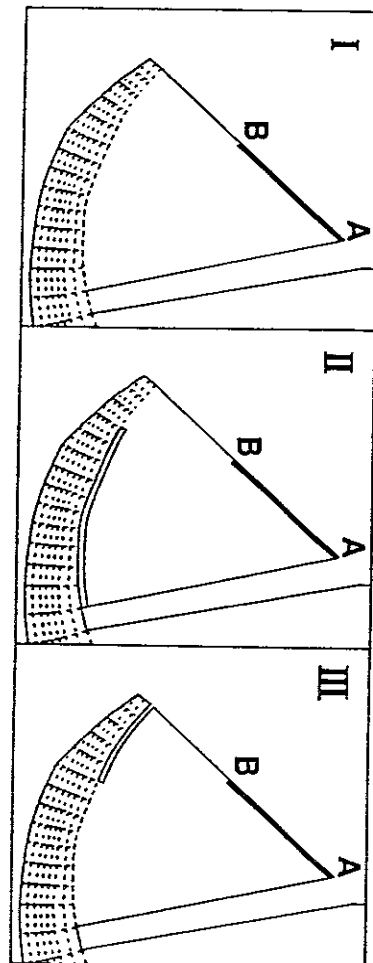


Fig. 6

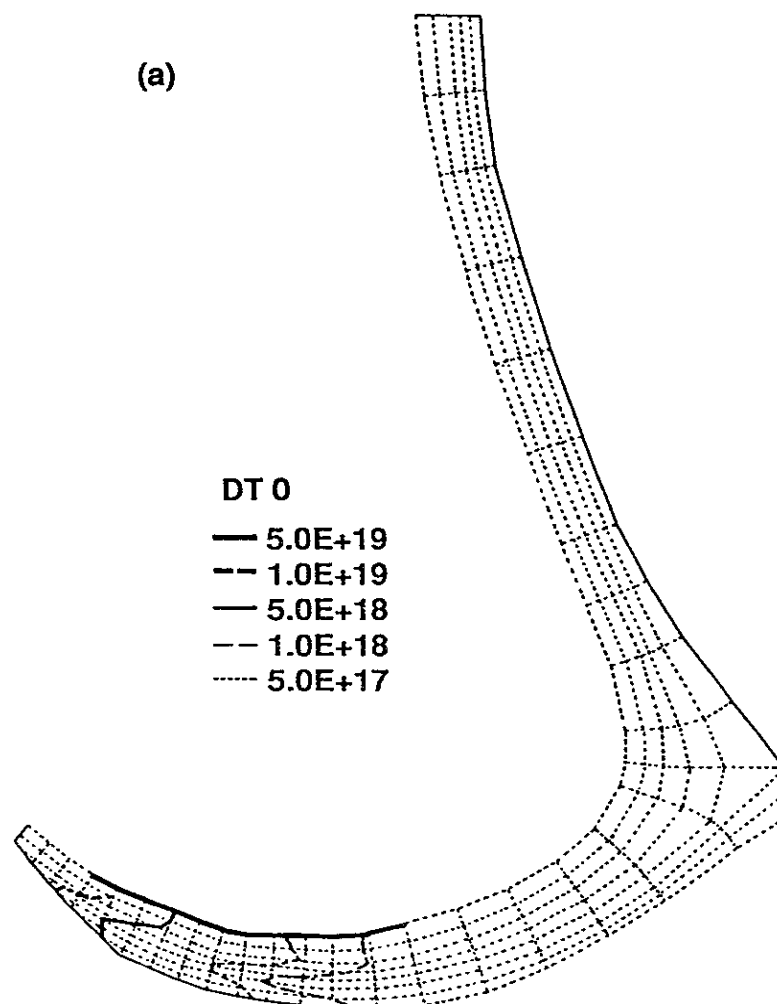


Fig. 6

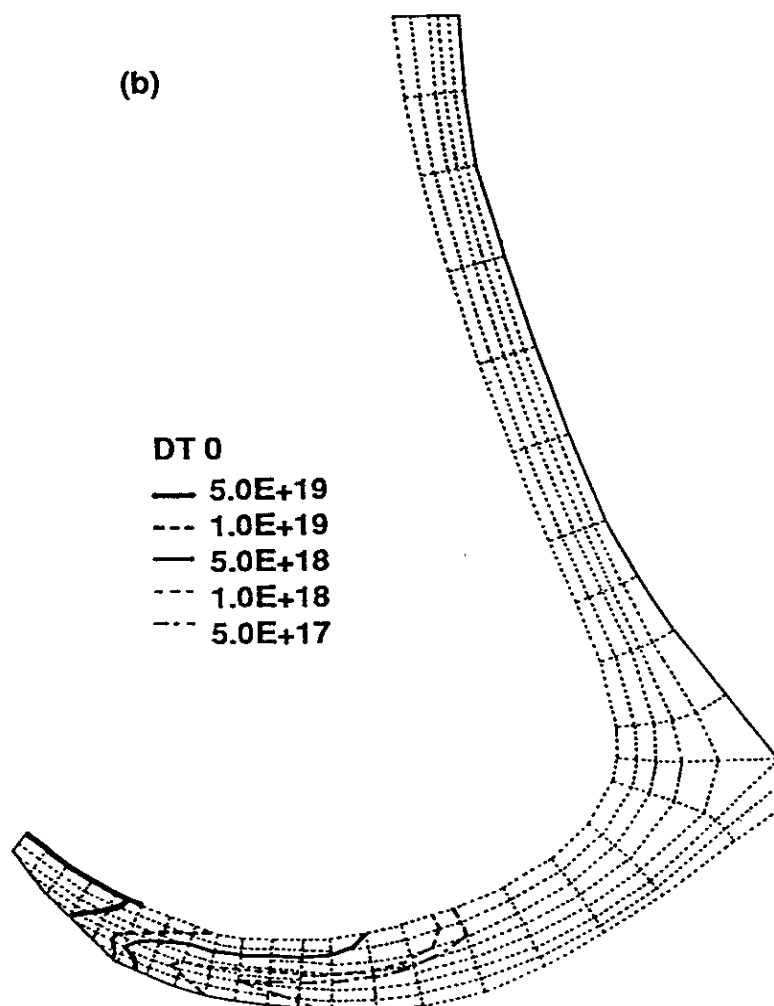


Fig. 6

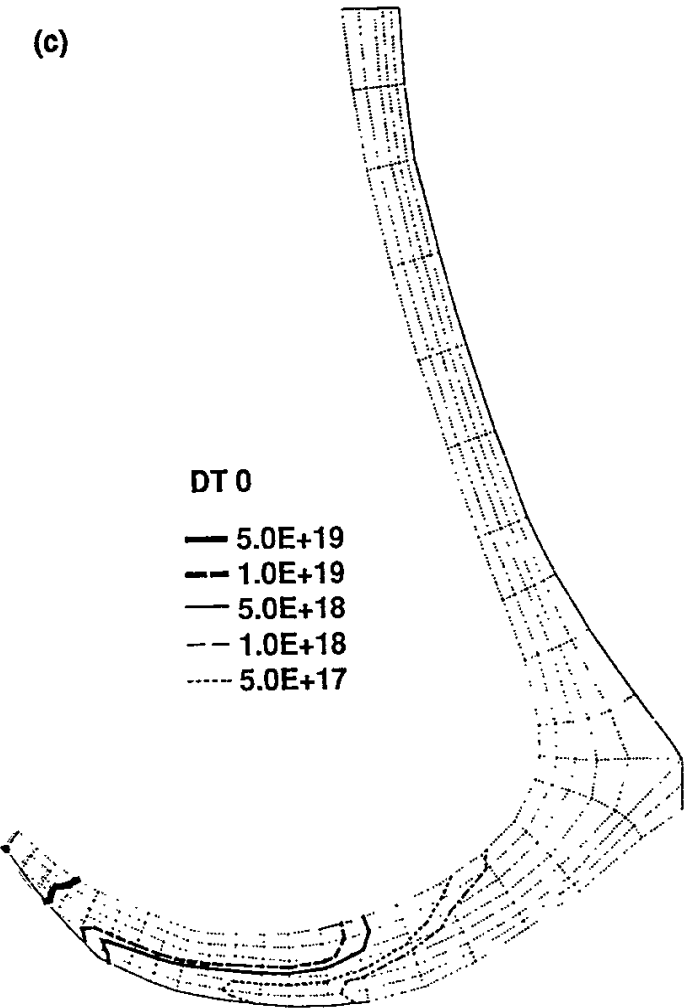
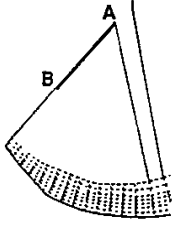
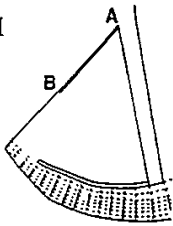
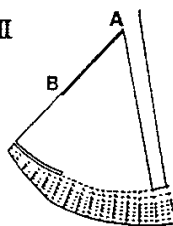
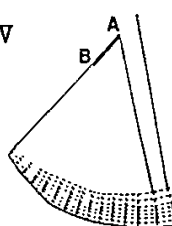


Table 1. Numerical Results

| Type | Standard | 2 nd type | 3 rd type | Reduced pump |
|---|---|---|---|---|
| Shape | I  | II  | III  | IV  |
| $T_e^b/T_i^b(\text{eV})$ | 27/60 | 37/80 | 27/62 | 26/53 |
| $T_e^d/T_i^d(\text{eV})$ | 12/8 | 33/46 | 4/4 | 6/5 |
| $N^b (\text{m}^{-3})$ | 3×10^{19} | 2×10^{19} | 3×10^{19} | 4.5×10^{19} |
| $N^d (\text{m}^{-3})$ | 9×10^{19} | 3×10^{19} | 30×10^{19} | 30×10^{19} |
| $\Sigma \Gamma_d / \Sigma \Gamma_p$ | ~ 12 | ~ 3 | 25 | 25 |
| $\Sigma \Gamma_{\text{pump}} (\text{s}^{-1})$ | $\sim 4 \times 10^{22}$ | 6×10^{22} | 8×10^{21} | 2×10^{22} |
| $\Sigma \Gamma_{\text{in}}^0 (\text{s}^{-1})$ | 1.6×10^{22} | 4×10^{21} | 4×10^{21} | 1×10^{22} |
| $\Sigma \Gamma_d (\text{s}^{-1})$ | 1×10^{24} | 3×10^{23} | 2×10^{24} | 2×10^{24} |
| Peak erosion (m/y) | ~ 1.2 | ~ 1.4 | ≤ 0.1 | 0.3-0.4 |
| Remark | <ul style="list-style-type: none"> • high T_e^d & low N_e^d • high erosion • Bad divertor function | <ul style="list-style-type: none"> • very high T_e^d & very low N_e^d • high erosion • Bad divertor function | <ul style="list-style-type: none"> • very low T_e^d & high N_e^d • negligible erosion • good divertor function | <ul style="list-style-type: none"> • low T_e^d & high N_e^d • low erosion • reasonable divertor function |